Accepted Manuscript

CFDsimulation of nanofluid forced convection inside a three-dimensional annulus by two-phase mixture approach: heat transfer and entropy generation analyses

Arash Rezaei Gorjaei , M. Soltani , Mehdi Bahiraei , Farshad M. Kashkooli

PII: S0020-7403(18)30943-3
DOI: https://doi.org/10.1016/j.ijmecsci.2018.08.002
Reference: MS 4460

To appear in: *International Journal of Mechanical Sciences*

Received date: 23 March 2018
Revised date: 5 July 2018
Accepted date: 3 August 2018

Please cite this article as: Arash Rezaei Gorjaei , M. Soltani , Mehdi Bahiraei , Farshad M. Kashkooli , CFDsimulation of nanofluid forced convection inside a three-dimensional annulus by two-phase mixture approach: heat transfer and entropy generation analyses, *International Journal of Mechanical Sciences* (2018), doi: https://doi.org/10.1016/j.ijmecsci.2018.08.002

Highlights

- Two-phase mixture model is used to solve nanofluid forced convection in 3D annulus.
- Annulus walls are subjected to constant and same temperature boundary condition.
- Both first and second laws of thermodynamics are considered.
- Concentration at upper side of inner cylinder is greater than other regions.

CFD simulation of nanofluid forced convection inside a three-dimensional annulus by two-phase mixture approach: heat transfer and entropy generation analyses

Arash Rezaei Gorjaei[a], M. Soltani[a,b,c,*], Mehdi Bahiraei[d], Farshad M. Kashkooli[a]

[a] Department of Mechanical Engineering, K. N. Toosi University of Technology, Tehran, Iran

[b] Department of Earth & Environmental Sciences, University of Waterloo, Waterloo, Ontario, Canada

[c] Waterloo Institute for sustainable energy (WISE), University of Waterloo, Waterloo, Ontario, Canada

[d] Department of Mechanical Engineering, Kermanshah University of Technology, Kermanshah, Iran

[*]Corresponding author

Corresponding author: M. Soltani, Assistant Professor at Department of Mechanical Engineering, K. N. Toosi University of Technology, Tehran, Iran & Department of Earth Environmental Sciences, University of Waterloo, Waterloo, Ontario, Canada &. msoltani@uwaterloo.ca, Tel./Fax: +1 (519) 8884567.

Abstract

The behavior of water–Al_2O_3 nanofluid inside the three-dimensional horizontal concentric annulus is investigated by the two-phase mixture procedure regarding the first and second laws of thermodynamics. The annulus walls are subjected to constant temperature boundary condition. Heat transfer and entropy generation rates, nanoparticle distribution, skin friction coefficient, and temperature distribution are evaluated at different concentrations and Reynolds numbers. The results show that nanoparticle concentration at the bottom of annulus and the upper side of inner cylinder is greater than other regions. In addition, the heat transfer and thermal entropy generation rates increase with increment of concentration and Reynolds number. Moreover, the

lowest and highest thermal entropy generation rates happen in the annulus central part and near the walls, respectively. Bejan number is very close to 1 at all cases under study, which shows the dominance of thermal entropy generation.

Keywords: Annulus, nanofluid, two-phase mixture model, forced convection, entropy generation.

Nomenclature

Be	Bejan number
C_p	specific heat (J/kgK)
D_h	hydraulics diameter (= D_0-D_i) (m)
d_f	diameter of base fluid molecular (m)
d_p	diameter of solid phase (m)
g	gravitational acceleration (m/s^2)
K_B	Boltzmann constant (=1.3807 / 10^{23}) (J/K)
k	thermal conductivity (W/mK)
L	length (m)
$\dot{m}$	mass flow rate (=$\rho_m V_{in} A$) (kg/s)
P	pressure (Pa)
Re	Reynolds number (=$\rho_m V_{in} D_h / \mu_m$)
$\dot{s}_t$	thermal EG rate (W/K)
$\dot{s}_f$	frictional EG rate (W/K)
T	temperature (K)
V	velocity (m/s)
V_B	the Brownian velocity of solid phases (m/s)

Greek letters

α	thermal diffusivity (m^2/s)
λ_f	average free path of base fluid molecular (=0.17) (nm)
δ	the distance between solid phases (m)
η	variable
μ	dynamic viscosity (Ns/m^2)
ν	kinematics viscosity (m^2/s)
ρ	density (kg/m^3)
τ	shear stress (N/m^2)
ϕ	concentration

Subscripts

dr	drift
f	fluid
h	hot
in	inlet
i	inner cylinder
m	mixture
n	the number of phases
out	outlet
o	outer cylinder
p	particle (solid phase)

1. Introduction

Nanofluids are novel kind of suspensions introduced by Choi in 1995 [1] which consist of well-dispersed solid nanometer-sized particles [2, 3]. Experiments have proven that with addition of nanoparticles, thermo-physical properties of base fluids including density, viscosity, and thermal conductivity increase [4]. The high thermal conductivity of these particles compared with that of the base fluids can enhance the heat transfer rate in many practical applications like heat exchangers, thermal storage systems, solar collectors, electronics cooling, and so forth [5-8].

Many studies have been performed for investigating the forced convection heat transfer of nanofluids [9-12]. For simulation of nanofluids flow, the single-phase and two-phase models could be used. The single-phase model is easier and has less computational time. This model considers the fluid and particles motion with the same velocity and also, they are assumed in thermal equilibrium. The single-phase model has been utilized in many numerical investigations of nanofluids flow [13-17]. On the other hand, many parameters like gravity, sedimentation, fluid and solid particles friction, and Brownian diffusion may influence a nanofluid flow. Two-phase models have better prediction in nanofluid flow investigation and also, take into account the solid and fluid molecular movements. Lotfi et al. [18] examined the flow of nanofluid in circular tube with three various models (single-phase, two-phase mixture, and two-phase Eulerian). The results demonstrated that the second one is more accurate than the other models. Recently, two-phase mixture model has been utilized to predict the nanofluids behavior by some researchers [19-24]. Behzadmehr et al. [23] investigated flow of the Cu–water nanofluid through a tube using the two-phase mixture procedure. Esmaeilnejad et al. [11] numerically studied forced convection within rectangular microchannels. In their study, the two-phase mixture

approach was used to investigate the flow behavior of a non-Newtonian nanofluid. Ghaffari et al. [24] studied nanofluid flow inside curved tubes with two-phase mixture model. The effects of parameters such as centrifugal force, buoyancy force and volume fraction of solid phase were studied.

The annular conduits are significant geometries for heat exchange and fluid flow devices. They have many applications in engineering including turbo-machinery, double-pipe heat exchangers, solar collectors, nuclear reactors, chemical industries, and so on. Hence, considerable research has been carried out in the case of concentric and eccentric circular annuli with constant heat flux or constant temperature boundary conditions. Izadi et al. [25] examined forced convection of water–Al_2O_3 nanofluid in a 2-D concentric annulus with considering the boundary condition of constant heat flux. Moghari et al. [26] researched the mixed convection of the Al_2O_3–water nanofluid in concentric annulus under the constant heat flux at the walls. The results indicated that at the specific Reynolds and Grashof numbers, increasing nanoparticle concentration enhances the Nusselt number at the inner and outer walls while it has no considerable impact on the friction factor. Natural heat transfer of a hybrid nanofluid in 2D eccentric horizontal cylindrical annulus was evaluated by Tayebi and Chamkha [27]. It was concluded that use of the Cu–Al_2O_3/water hybrid nanofluid provides a better thermal and hydrodynamic efficiency in comparison with the Al_2O_3/water nanofluid.

To investigate the nanofluid flow, the first and second laws of thermodynamics can be considered. The minimum entropy generation can be obtained by applying the second law of thermodynamics in engineering problems. Several researchers have applied the second law of thermodynamics for studying the nanofluid attributes [28-30]. Mahian et al. [31] conducted a comprehensive review on entropy generation in nanofluid flow. Bianco et al. [32] studied

turbulent nanofluid flow and entropy generation inside a circular pipe under constant temperature boundary condition. They showed as nanofluid volume fraction increases, pumping power and entropy generation intensify. Bahiraei and Mohammadi Majd [33] investigated the water–Al_2O_3 nanofluid flow within a triangular minichannel, while the constant wall heat flux was considered as boundary condition. Their results demonstrated that by the increase of the particle size, total entropy generation and Bejan number increases and reduces, respectively.

According to the presented literature survey and to the best knowledge of the authors, forced convection of nanofluids inside three-dimensional concentric annuli under constant temperature boundary condition has not been investigated so far via two-phase methods. In the current research, the first and second laws of thermodynamics are considered. The significant parameters including skin friction coefficient, heat transfer rate, temperature distribution, entropy generation rates as well as nanoparticle distribution are investigated and discussed in detail.

2. Description and formulation of the model

2.1. Two-phase mixture procedure

The two-phase mixture procedure is employed with considering the fact that the coupling between phases is strong. In two-phase mixtures, many parameters like gravity, sedimentation, fluid and solid particles friction, and Brownian diffusion may influence behavior of mixtures. Consequently, for simulation of nanofluid flows, the slip velocity between the fluid and particles must be considered. Generally, two-phase models present better prediction for flow of nanofluids, and take into account solid and fluid interactions [26]. In this approach, instead of the separate equations for each phase, the governing equations are utilized for the mixture. These equations are as follows:

- Continuity:

$$\nabla.(\rho_m \vec{V}_m) = 0 \quad (1)$$

- Momentum:

$$\nabla.(\rho_m \vec{V}_m \vec{V}_m) = -\nabla P + \nabla.(\mu_m \nabla \vec{V}_m) + \nabla. \sum_{s=1}^{n} (\phi_s \rho_s \vec{V}_{dr,s} \vec{V}_{dr,s}) + \rho_m g \quad (2)$$

- Energy:

$$\nabla. \sum_{s=1}^{n} (\phi_s \rho_s \vec{V}_s T C_{p,s}) = \nabla.(k_m \nabla T) \quad (3)$$

- Volume fraction:

$$\nabla.(\phi_p \rho_p \vec{V}_m) = -\nabla.(\phi_P \rho_P \vec{V}_{dr,p}) \quad (4)$$

The mixture velocity is obtained by:

$$\vec{V}_m = \frac{\sum_{s=1}^{n} \phi_s \rho_s \vec{V}_s}{\rho_m} \quad (5)$$

$\vec{V}_{dr,p}$ and $\vec{V}_{pf}$ are respectively the drift velocity (between nanoparticles and mixture) and the relative velocity (between nanoparticles and base fluid).

$$\vec{V}_{dr,p} = \vec{V}_p - \vec{V}_m \quad (6)$$

$$\vec{V}_{pf} = \vec{V}_p - \vec{V}_f \quad (7)$$

where *f* and *p* refer to base fluid and nanoparticles, respectively.

The drift velocity is associated to the relative velocity:

$$\vec{V}_{dr,p} = \vec{V}_{pf} - \sum_{s=1}^{n} \frac{\phi_s \rho_s}{\rho_m} \vec{V}_{fs} \tag{8}$$

The relative velocity ($\vec{V}_{pf}$) and drag coefficient (f_{drag}) are defined respectively by Manninen et al. [34] and Schiller and Naumann [35].

$$\vec{V}_{pf} = \frac{\rho_p d_p^2}{18\mu_f f_{drag}} \frac{(\rho_p - \rho_m)}{\rho_p} \vec{a} \tag{9}$$

where a is acceleration ($\vec{a} = (\vec{g} - (\vec{V}_m.\nabla)\vec{V}_m)$).

$$f_{drag} = \begin{Bmatrix} 1 + 0.15\,\mathrm{Re}_p^{0.687}, \mathrm{Re}_p \le 1000 \\ 0.0183\,\mathrm{Re}_p, \mathrm{Re}_p > 1000 \end{Bmatrix}, \quad \mathrm{Re}_p = \frac{V_m d_p}{\upsilon_m} \tag{10}$$

where υ_m and d_p are kinematics viscosity of mixture and nanoparticles diameter, respectively.

2.2. Definition of geometry and boundary conditions

The geometry under study (i.e. horizontal concentric annulus) is demonstrated in Fig. 1. Radiuses of two cylinders are r_i and r_o (r_o = 2r_i), and the annulus length is equal to 15D_h (L = 15D_h). The gravitational force is exerted in the vertical direction.

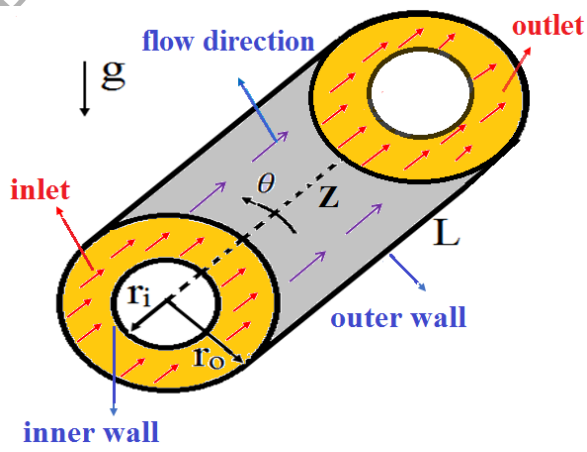

Fig. 1. Geometry under study and relevant coordinate system.

The problem's boundary conditions are as follows:

- At the annulus inlet, the flow velocity is only in the *z* direction. In two other directions, the flow velocity is zero. Also, at the annulus inlet, the flow temperature is uniform and constant. Therefore, at the inlet:

$$V_{\mathrm{m,z}} = V_{\mathrm{in}},\ V_{\mathrm{m,r}} = V_{\mathrm{m},\theta} = 0 \quad \text{and} \quad \mathrm{T} = \mathrm{T_{in}} \tag{11}$$

- For the walls of the annulus, no-slip condition is applied (in three directions, the flow velocity is zero). The temperature of walls is constant and uniform (T_h):

Hence, at the walls:

$$V_{\mathrm{m,z}} = V_{\mathrm{m,r}} = V_{\mathrm{m},\theta} = 0 \quad \text{and} \quad T_h = 320\ \mathrm{K} \tag{12}$$

- At the annulus outlet, a zero relative pressure is considered.

$$P = P_{atm} \tag{13}$$

2.3. Properties of nanofluid

In Table 1, the properties of nanoparticle (Al_2O_3) and base fluid (water) are given. The nanoparticles diameter is 72 nm and they are spherical, and are similar in scale and form.

Table 1. Thermophysical properties of Al_2O_3 and water [6].

Properties	Water	Nanoparticles (Al_2O_3)
ρ (kg/m^3)	997.1	3970
μ (kg/ms)	0.000855	-
C_p (J/kgK)	4179	765

k (W/mK)	0.613	40

The utilized equations for calculating nanofluid properties are as follows:

ρ_m and $C_{p,m}$ are obtained as:

$$\rho_m = (1 - \phi)\rho_f + \phi\rho_p \tag{14}$$

$$C_{p,m} = \frac{(1-\phi)\rho_f C_{p,f} + \phi\rho_p C_{p,p}}{\rho_m} \tag{15}$$

The following equation was suggested by Masoumi et al. [36] for dynamic viscosity:

$$\mu_m = \mu_f + \frac{\rho_p d_p{}^2 V_B}{72\delta C} \tag{16}$$

where V_B, δ and C are obtained by the following equations:

$$V_B = \frac{1}{d_p}\sqrt{\frac{18K_B T}{\pi\rho_p d_p}} \tag{17}$$

$$\delta = \sqrt[3]{\frac{\pi}{6\phi}}d_p \tag{18}$$

$$C = \mu_f^{-1}[(C_1 d_p + C_2)\phi + (C_3 d_p + C_4)] \tag{19}$$

where C_1, C_2, C_3 and C_4 are given as:

$C_1 = -1133$, $C_2 = -0.000002771$, $C_3 = 90$, $C_4 = -0.000000393$ (20)

The following equation was offered by chon et al. [37] for thermal conductivity:

$$\frac{k_m}{k_f} = 1 + 64.7\phi^{0.746}\left(\frac{d_f}{d_p}\right)^{0.369}\left(\frac{k_P}{k_f}\right)^{0.7476}\mathrm{Pr}_f{}^{0.9955}\,\mathrm{Re}_f{}^{1.2321} \tag{21}$$

where Pr_f and Re_f are obtained by following equations:

$$\mathrm{Pr}_f = \frac{\eta}{\rho_f \alpha_f} \tag{22}$$

$$\mathrm{Re}_f = \frac{\rho_f K_B T}{3\pi \eta^2 \lambda_f} \tag{23}$$

where η is obtained as:

$$\eta = B.10^{\frac{A}{T-H}} \text{ in which } B = 2.414\times10^{-5},\ A = 247.8,\ H = 140 \tag{24}$$

2.4. Definition of parameters

Heat transfer rates for the nanofluid and the skin friction coefficient on the walls are calculated respectively by the following equations:

$$\dot{q} = \dot{m} C_{p,m} (T_{out} - T_{in}) \tag{25}$$

$$C_{f,i} = \frac{\tau_i}{0.5\rho_m V_{in}^2} \quad \text{and} \quad C_{f,o} = \frac{\tau_o}{0.5\rho_m V_{in}^2} \tag{26}$$

where τ is calculated on the inner and outer walls as below:

$$\tau_i = \mu_m (\frac{\partial V_r}{\partial r})_i \quad \text{and} \quad \tau_o = \mu_m (\frac{\partial V_r}{\partial r})_o \tag{27}$$

The total entropy generation rate is obtained as:

$$\dot{S}''' = \dot{S}_t''' + \dot{S}_f''' \tag{28}$$

where $\dot{S}_t'''$ and $\dot{S}_f'''$ are thermal and frictional entropy generation rates, respectively.

$$\dot{S}_t''' = \frac{k_m}{T^2}[(\frac{\partial T}{\partial x})^2 + (\frac{\partial T}{\partial y})^2 + (\frac{\partial T}{\partial z})^2] \tag{29}$$

$$\dot{S}_f''' = \frac{\mu_m}{T}\left\{2[(\frac{\partial u}{\partial x})^2 + (\frac{\partial v}{\partial y})^2 + (\frac{\partial w}{\partial z})^2] + (\frac{\partial u}{\partial y} + \frac{\partial v}{\partial x})^2 + (\frac{\partial u}{\partial z} + \frac{\partial w}{\partial x})^2 + (\frac{\partial w}{\partial y} + \frac{\partial v}{\partial z})^2\right\} \tag{30}$$

With integrating from Eqs. (29) and (30) on the whole volume, global thermal entropy generation rate and global frictional entropy generation rate are obtained.

$$\dot{S} = \int \dot{S}''' d\forall \tag{31}$$

To evaluate the contribution of heat transfer and friction in the entropy generation, a non-dimensional number (i.e. Bejan number), which is the ratio of thermal entropy generation rate to total entropy generation rate, is defined as:

$$Be = \frac{\dot{S}_t}{\dot{S}} \tag{32}$$

3. Numerical procedure and validation

In this simulation, the coordinates are in three directions (Z-θ-r), and the suitable combination of meshes is selected in all directions. With increasing the number of cells in three directions (the size of the meshes), it is tried to find the optimal mesh for this geometry. Fig. 2 shows one instance of structured grids listed in Table 2. It is demonstrated that the grid containing 55, 55 and 55 cells respectively in the *Z* (axial), θ (tangential) and *r* (radial) directions is the optimal grid. This is because increasing the number of cells (in three directions) does not change significantly the heat transfer rate compared with the mentioned grid.

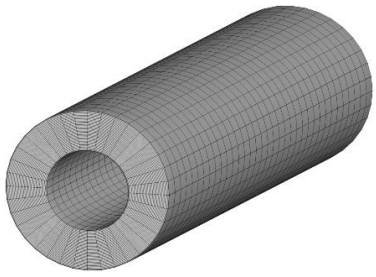

Fig. 2. Structured grid type.

Table 2. Mesh independency at ϕ = 0.02, *Re* = 600.

Grid numbers (*Z*-θ-*r*)	Heat transfer rate (W)

30-30-30	90.21
35-35-35	101.82
40-40-40	108.61
45-45-45	114.36
50-50-50	118.02
55-55-55	**120.25**
60-60-60	120.56
65-65-65	120.97

The finite volume technique is used for solving the governing equations (continuity, momentum, energy, and volume fraction). For coupling the pressure and velocity, SIMPLEC method is utilized and also, the second order upwind procedure is employed for Eqs. (2) and (3) [38].

In order to ensure the validity of the numerical procedure, the results of the present research are compared with two different studies including one experimental work and one numerical investigation. The selected parameters include the Nusselt number (Nu) and skin friction coefficient (C_f) reported by Mirmasoumi and Behzadmehr [21] at Re = 300, d_p =10 nm, ϕ = 0.04 and Ri=1 (numerical work); and the local convective heat transfer coefficient (h) on the tube wall with the length of 1 m at flow rate of 2.6 L/min and ϕ = 0.02 reported by Sheikhnejad et al. [39] (experimental work). As can be seen from Fig. 3, there is a proper consistency between the results of present numerical work and the above-mentioned studies. It is noteworthy that the average deviations of present work's results in compression with the numerical work and experimental study are 1.5% and 4%, respectively.

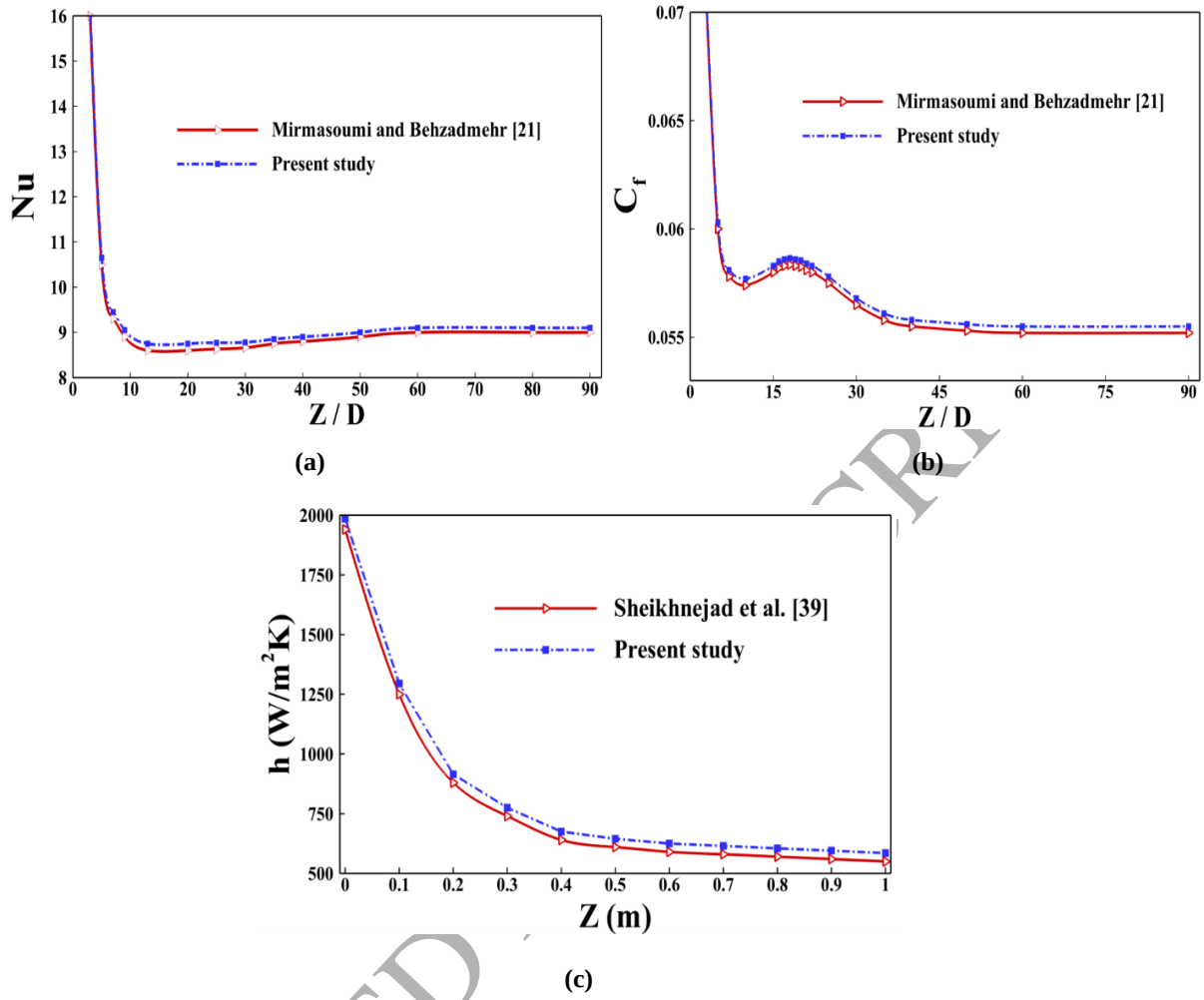

Fig. 3. Comparison between the results of present study with: (a) and (b) numerical work of Mirmasoumi and Behzadmehr [21], (c) experimental work of Sheikhnejad et al. [39].

4. Results and discussion

The current research investigates the forced convective heat exchange and entropy generation of the water–Al_2O_3 nanofluid within the horizontal concentric annulus by the two-phase mixture approach. Constant and uniform temperature boundary conditions on the annulus walls (T_i = T_o = T_h) are applied. The annulus aspect ratio and its length (L) are 2 and 15D_h, respectively. Various concentrations and Reynolds numbers are considered to evaluate the thermal and hydrodynamic attributes of the nanofluid. The local skin friction coefficient, heat transfer rate

(q), entropy generation rates, nanoparticle distribution, and temperature profile are obtained and discussed at five following sections in details.

4.1. Nanoparticle distribution

The nanoparticle distribution at the annulus outlet is illustrated at Re = 600 for different concentrations in Fig. 4, and at ϕ = 0.05 for different Reynolds numbers in Fig. 5. The temperature conditions (constant, uniform and same), nanofluid flow (forced convection), and the geometry under study are symmetrical. Therefore, uniform distributions for the nanoparticles are observed at the left and right surfaces of the annulus outlet. However, Figs. 4 and 5 show that the gravity force affects the distribution of nanoparticles in the annulus. In this regard, concentration of solid phase at the outer wall's bottom side and the upper side of the inner wall has increased. On the contrary, solid phase concentration at the outer wall's upper side and at the lower side of the inner wall has reduced. Besides, at the annulus center, the solid phase distribution is constant and uniform. The results reveal that at higher concentrations, the sedimentation increases compared to the initial value. It can be concluded from Fig. 5 that the Reynolds number and gravity force also affect the sedimentation of solid phase. In this situation, increment of Reynolds number means the nanofluid velocity increase and therefore, the solid phase sedimentation decreases at the bottom of the annulus.

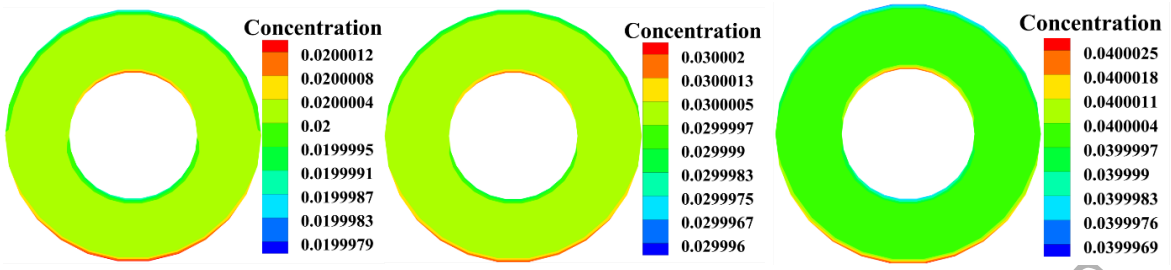

(a) ϕ = 0.02 (b) ϕ = 0.03 (c) ϕ = 0.04

Fig. 4. Solid phase distribution for different concentrations at *Re* = 600.

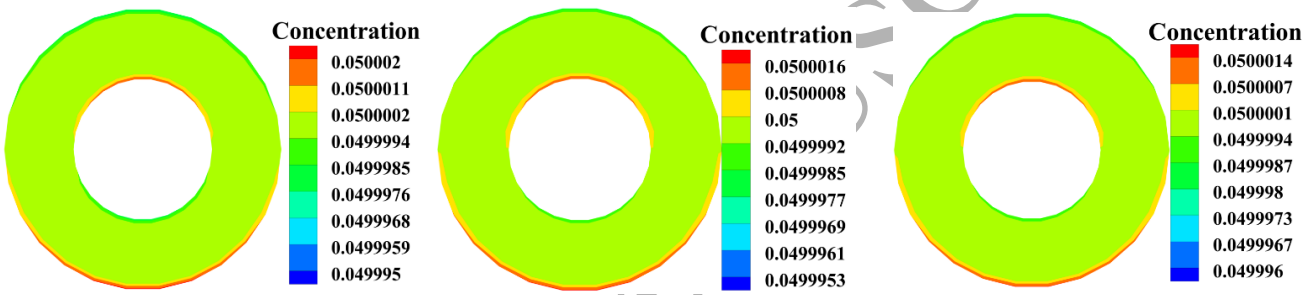

(a) *Re* = 900 (b) *Re* = 1200 (c) *Re* = 1500

Fig. 5. Solid phase distribution for different Reynolds numbers at ϕ = 0.05.

Fig. 6 shows the solid phase distribution within the annulus at *Re* = 900 and ϕ = 0.05. It is found that due to the gravity force, the concentration respectively increases and decreases at the bottom and the top of the annulus. As can be observed, the sedimentation increases (at the bottom of the annulus) along the annulus. In fact, the boundary layer grows along the annulus and affects the slip between the two phases. Based on the results obtained, it can be concluded that the solid phase sedimentation strongly depends on the gravity force, Reynolds number, and concentration.

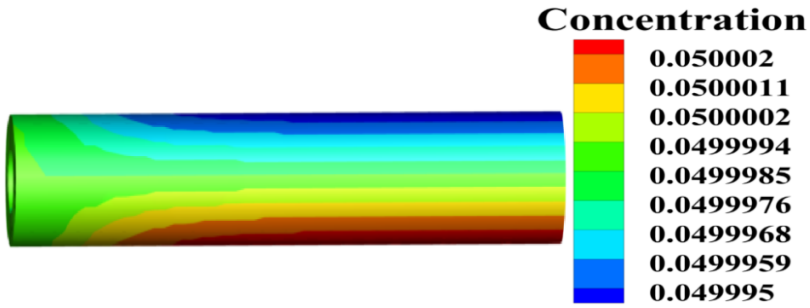

Fig. 6. Solid phase distribution inside the annulus at Re = 900 and ϕ = 0.05.

4.2. Local skin friction coefficient

The effect of the solid phase concentration on local skin friction coefficients ($C_{f,i}$ and $C_{f,o}$) is shown in Fig. 7 for Re = 600. Increase of concentration leads to increase of the nanofluid density and decrease of the velocity gradient. Therefore, with respect to Eqs. (26) and (27), increment of the concentration leads to decrement in skin fraction coefficient on the walls. It should be noted that with the concentration increment, the velocity and viscosity decreases and increases, respectively. The skin friction coefficients on both walls at annulus entrance possess higher values in comparison with the region in which $L > 1\times D_h$. This is because that in the entrance region, the maximum velocity gradient occurs. Fig. 8 illustrates the non-dimensional velocity distribution inside the half of annulus for ϕ = 0.02 and Re = 600. It is seen that the hydrodynamic boundary layer is thinner in the annulus entrance and therefore, the maximum velocity gradients happen there.

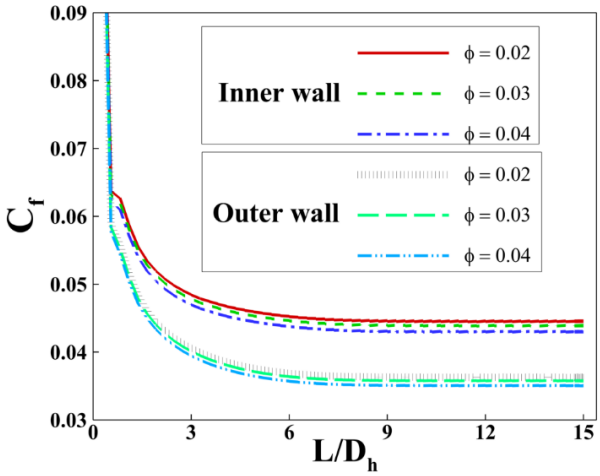

Fig. 7. Concentration effects on local skin friction coefficient at *Re* = 600.

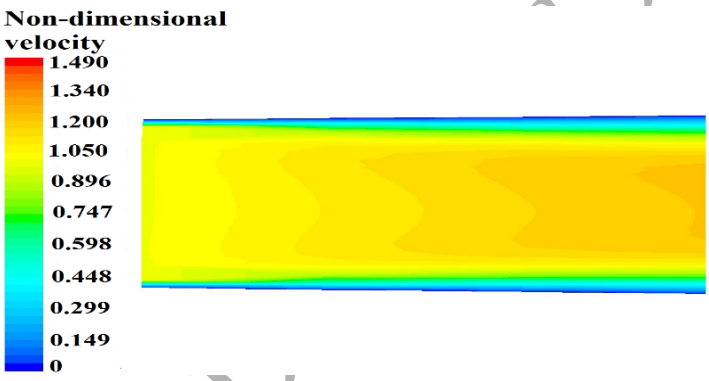

Fig. 8. Non-dimensional velocity distribution inside half of annulus at ϕ = 0.02 and *Re* = 600.

Investigation of the Reynolds number effect on local skin friction coefficients is depicted in Fig. 9 for ϕ = 0.05. The local skin friction coefficient decreases with enhancement of the Reynolds number because the Reynolds number increment increases the nanofluid velocity, which leads to a higher dynamic pressure. Moreover, it is obvious that the slope of friction coefficients decreases quickly, and becomes approximately invariant near the inlet. This indicates that the growth of the hydrodynamic boundary layer is significant.

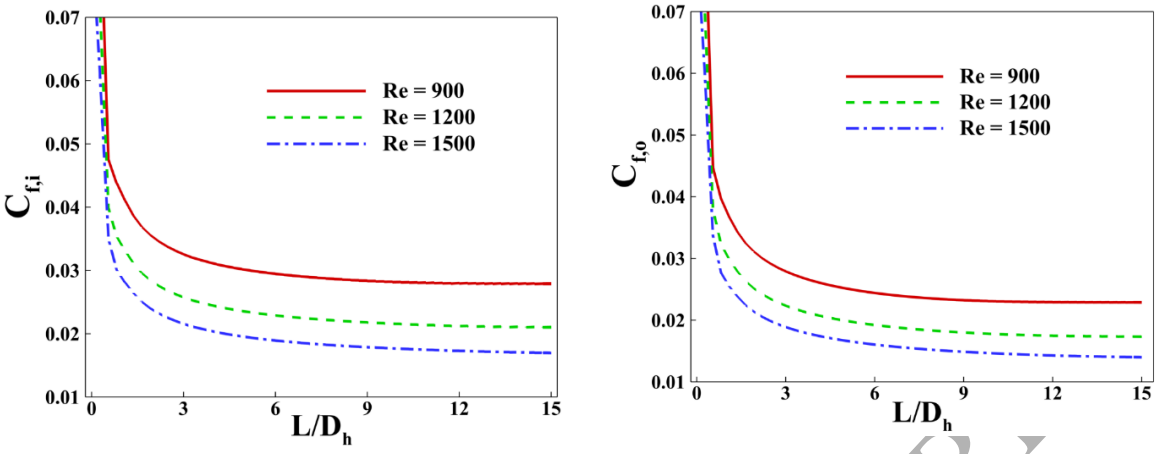

Fig. 9. Reynolds number effects on local skin friction coefficient for *Re* = 900, 1200 and 1500 at ϕ = 0.05.

Figs. 7 and 9 demonstrate that the local skin friction factor on the outer wall has the lower values in comparison with the corresponding values on the inner wall. The reason is that the outer wall has a milder curvature and therefore, velocity gradient on the outer wall is smaller than that on the inner wall.

4.3 Heat transfer rate

Table 3 summarizes the heat transfer rates for different concentrations and Reynolds numbers. It can be noticed that the heat transfer augments with the concentration increment. This is because the outlet temperature and density of nanofluid increase by enhancing concentration. While, in this case, the velocity and specific heat of the nanofluid are decreased. Physically, the reason of heat transfer enhancement with the concentration increment is increase of the nanofluid thermal conductivity, which intensifies the convective heat transfer coefficient. As can be observed, the heat transfer rate also enhances with an increase in Reynolds number. Indeed, Reynolds number increment means an increase in the nanofluid velocity whereas the outlet

temperature reduces. In effect, the mass flow rate is greater for higher Reynolds numbers, and physically, the thermal boundary layer is thinner.

Table 3. Heat transfer rates for several values of *Re* and ϕ.

Re = 600	ϕ	0.02	0.03	0.04
	q (W)	120.25	155.72	175.80
ϕ = 0.05	*Re*	900	1200	1500
	q (W)	229.44	257.51	282.38

4.4. Temperature distribution

In the current paper, the heat transfer mechanism is forced convection and therefore, the temperature distribution inside the annulus is symmetrical. As a result, only one half of the annulus is presented. Fig. 10 shows distribution of the nanofluid temperature for Reynolds numbers of 100 and 200 with concentration of 4% in the annulus half. The temperature of inner and outer walls of the annulus are constant, uniform and same (T_h = 320 K). Also, at the annulus inlet, the temperature of nanofluid is uniform and constant (T_{in} = 300 K, see Fig. 11a). The nanofluid temperature increases along the annulus, and its value at *Re* = 200 is much lower than that at *Re* = 100. This is because at *Re* = 200, the nanofluid velocity is greater and therefore, the thickness of the thermal boundary layer is smaller. In addition, the residence time of the flow is lower for the higher Reynolds number. It is found that the nanofluid flow develops at $L \cong 14\ D_h$ for *Re*=100 whereas the flow development occurs at $L > 15\ D_h$ for *Re*=200. Therefore, for *Re* = 100 at the annulus outlet, the temperature value is approximately 320 K (see Fig. 11b). While, for *Re* = 200, the temperature value is different (see Fig. 11c). Also, it can be seen that due to the

greater surface of the outer cylinder than the inner cylinder, the more heat reaches the nanofluid flow from this cylinder. It is noteworthy that the temperature of both cylinders is same and uniform.

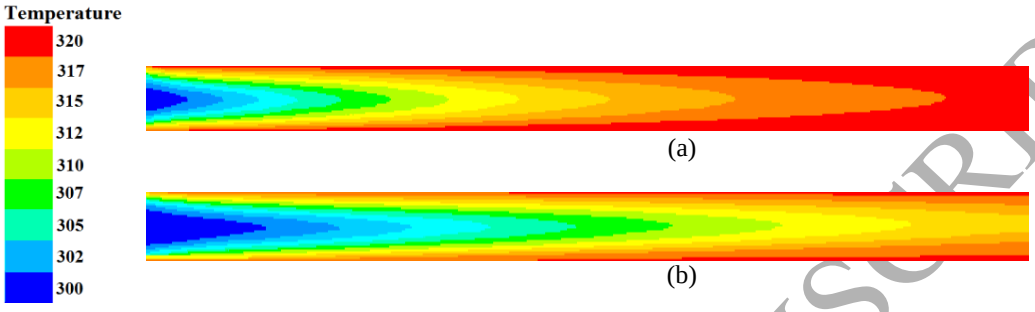

Fig. 10. Temperature distribution (K) inside the annulus half for ϕ = 0.04 at: (a) *Re*=100, (b) *Re*=200.

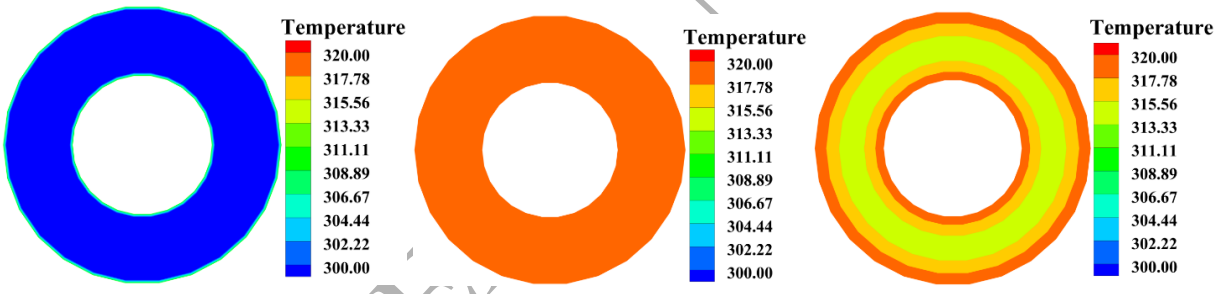

Fig. 11. Temperature distribution for ϕ = 0.04: (a) at annulus inlet, (b) at annulus outlet for *Re*=100, (c) at annulus outlet for *Re*=200.

4.5. Entropy generation rates

Table 4 (row *a*) shows global thermal and frictional entropy generation rates as well as Bejan number for *Re* = 600 at different concentrations. It is found that the frictional entropy generation rate reduces by increment of the concentration, because the velocity gradient and temperature

decreases and increases, respectively, while the nanofluid viscosity intensifies. In addition, the thermal entropy generation rate and Bejan number increase with the increment of concentration. The reason is that thermal condutivity enhances, and thermal boundary layer grows quicker with the concentration increment, which intensifies the global thermal entropy generation rate. Moreover, the value of Bejan number shows that the entropy generation due to the heat transfer is dominant because Bejan number is close to 1. Table 4 (row *b*) presents the global thermal and frictional entropy generation rates for different Reynolds numbers at ϕ = 0.05. It can be observed that the thermal and frictional entropy generation rates intensify as the Reynolds number increases. This is due to the fact that by increasing the Reynolds number, the velocity gradient intensifies while the nanofluid temperature decreases.

Table 4. Integrated rates of thermal and frictional entropy generation as well as Bejan number at different concentrations and Reynolds numbers.

a	*Re* = 600	ϕ	0.02	0.03	0.04
		$\dot{S}_t$ (W/K)	0.0216	0.0244	0.0271
		$\dot{S}_f \times 10^{-7}$ (W/K)	3.181	3.112	3.0813
		Be	0.9999852	0.9999872	0.9999886
b	ϕ = 0.05	*Re*	900	1200	1500
		$\dot{S}_t$ (W/K)	0.0359	0.0410	0.0452
		$\dot{S}_f \times 10^{-6}$ (W/K)	0.7213	1.3195	2.1131

Fig. 12 demonstrates the contour of thermal entropy generation rate for ϕ = 0.02 and *Re* = 600. Obviously, the more significant thermal entropy is generated near the annulus inlet

compared to near the annulus outlet. In fact, the thermal boundary layer is thinner at the region adjacent to the inlet. In addition, the lowest and highest thermal entropy generation rates happen respectively in the annulus central part and near the walls because the highest temperature gradients occur in the vicinity of the walls.

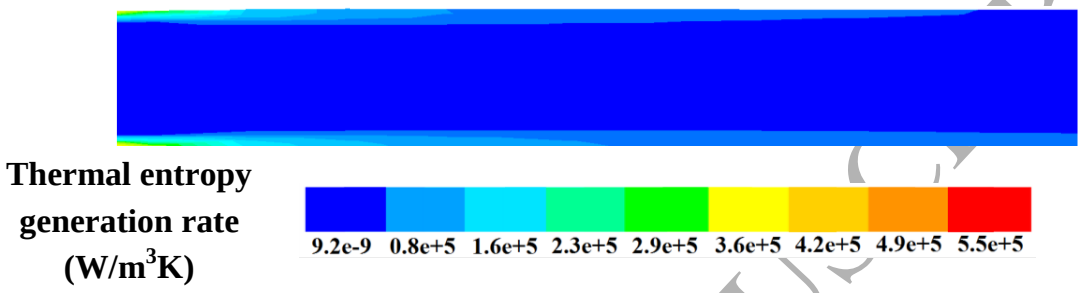

Fig. 12. Thermal entropy generation rate distribution inside the annulus half for ϕ = 0.02 and *Re* = 600.

The contour of local Bejan number at the cross section through center of the annulus is presented in Fig. 13 for ϕ = 0.02 and *Re* = 600. It is found that the value of Bejan number is very close to 1 in significant part of the annulus. In fact, there is a great temperature difference between the nanofluid and the annulus walls and therefore, noticeable thermal entropy is generated, which results in large Bejan numbers. It should be noted that the growth of the hydrodynamic boundary layer is faster than that of the thermal boundary layer and as can be seen at the beginning of the annulus, because the thermal boundary layer has not reached the central region, Bejan number is very small there due to very low temperature gradients. In addition, it is clear from the figure that with increase of the distance from the annulus inlet, Bejan number develops towards the central region thanks to the growth of thermal boundary layer.

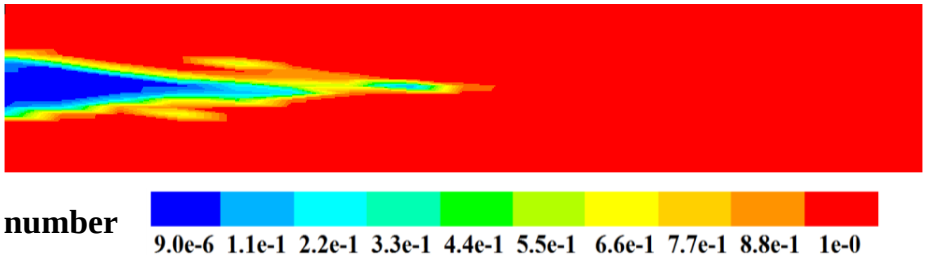

Fig. 13. Bejan number distribution at cross section through center of the annulus for ϕ = 0.02 and *Re* = 600.

5. Conclusion

In the present study, behavior of the water–Al_2O_3 nanofluid forced convection within the three-dimensional annulus is simulated via the two-phase mixture model regarding the first and second laws of thermodynamics. The walls of the annulus are subjected to constant temperature boundary condition. The heat transfer rate, second law attributes (i.e. thermal and frictional entropy generation rates as well as Bejan number), solid phase distribution, local skin friction coefficient, as well as the nanofluid temperature distribution are evaluated at different concentrations and Reynolds numbers. The major findings of the current investigation are as follows:

- Concentration of the solid phase increases at the bottom of the annulus and at the upper side of the inner cylinder. Moreover, the concentration decreases at the top of the annulus and at the lower side of the inner cylinder.
- Sedimentation of the solid phase at the bottom of the annulus decreases with increment of Reynolds number.
- The friction coefficients intensify by increasing the concentration, while decrease with the Reynolds number increment. Moreover, the friction coefficient on the outer wall has the less value compared to the inner wall and also, has much higher value at the annulus entrance.

- The nanofluid temperature increases along the annulus, and has much less value at higher Reynolds numbers. Moreover, at lower Reynolds numbers, the flow thermally develops at a location closer to the annulus inlet.
- Heat transfer rate enhances with increment of either concentration or Reynolds number.
- By increasing the Reynolds number, thermal and frictional entropy generation rates increase.
- As the solid phase concentration increases, thermal entropy generation rate and frictional entropy generation rate increases and decreases, respectively.
- Bejan number is very close to 1 at all states under study, which shows the dominance of thermal entropy generation.
- The lowest and highest thermal entropy generation rates happen in the annulus central part and near the walls, respectively.

References

[1] S. Choi, Enhancing thermal conductivity of fluids with nanoparticles, ASME-Publications-Fed., vol. 231, pp. 99–106, 1995.

[2] S.A.M. Mehryan, F.M. Kashkooli, M. Soltani, K. Raahemifar, Fluid flow and heat transfer analysis of a nanofluid containing motile gyrotactic micro-organisms passing a nonlinear stretching vertical sheet in the presence of a non-uniform magnetic field; numerical approach, PLOS ONE, 1 (2016) e0157598.

[3] S.A.M. Mehryan, F.M. Kashkooli, M. Ghalambaz, A.J. Chamkha, Free convection of hybrid Al_2O_3-Cu water nanofluid in a differentially heated porous cavity, Adv. Powder Technol., 28 (2017) 2295–2305.

[4] K. Bashirnezhad, M.M. Rashidi, Z. Yang, S. Bazri, W.M. Yan, A comprehensive review of last experimental studies on thermal conductivity of nanofluids, J. Therm. Anal. Calorim., 122 (2015) 863-884.

[5] W. Daungthongsuk, S. Wongwises, A critical review of convective heat transfer of nanofluids, Renew. Sust. Energ. Rev., 11 (2007) 797–817.

[6] A.J. Ahrar, M.H. Djavareshkian, Computational investigation of heat transfer and entropy generation rates of Al_2O_3 nanofluid with Buongiorno's model and using a novel TVD hybrid LB method, J. Mol. Liq., 242 (2017) 24–39.

[7] M. Bahiraei, R. Rahmani, A. Yaghoobi, E. Khodabandeh, R. Mashayekhi, M. Amani, Recent research contributions concerning use of nanofluids in heat exchangers: A critical review, Appl. Therm. Eng., 133 (2018) 137-159.

[7] V. Singh, M. Gupta, Heat transfer augmentation in a tube using nanofluids under constant heat flux boundary condition: a review, Energy Convers. Manage., 123 (2016) 290–307.

[8] M. Gupta, V. Singh, R. Kumar, Z. Said, A review on thermophysical properties of nanofluids and heat transfer applications, Renew. Sust. Energ. Rev., 74 (2017) 638–670.

[9] M. Bahiraei, K. Gharagozloo, M. Alighardashi, N. Mazaheri, CFD simulation of irreversibilities for laminar flow of a power-law nanofluid within a minichannel with chaotic perturbations: An innovative energy-efficient approach, Energy Convers. Manage., 144 (2017) 374–387.

[10] M. Bahiraei, Particle migration in nanofluids: A critical review, Int. J. Therm. Sci., 109 (2016) 90–113.

[11] A. Esmaeilnejad, H. Aminfar, M.Sh. Neistanak, Numerical investigation of forced convection heat transfer through microchannels with non-Newtonian nanofluids, Int. J. Therm. Sci., 75 (2014) 76-86.

[12] M. Bahiraei, M. Alighardashi, Investigating non-Newtonian nanofluid flow in a narrow annulus based on second law of thermodynamics, J. Mol. Liq., 219 (2016) 117–127.

[13] C.T. Nguyen, G. Roy, C. Gauthier, N. Galanis, Heat transfer enhancement using Al_2O_3 water nanofluid for an electronic liquid cooling system, Appl. Therm. Eng., 27 (2007) 1501–1506.

[14] M. Bahiraei, A. Rezaei Gorjaei, A. Shahidian, Investigating heat transfer and entropy generation for mixed convection of CuO–water nanofluid in an inclined annulus, J. Mol. Liq., 248 (2017) 36–47.

[15] J. Koo, C. Kleinstreuer, Laminar nanofluid flow in microheat-sinks, Int. J. Heat Mass Transf., 48 (2005) 2652–2661.

[16] M. Akbari, A. Behzadmehr, F. Shahraki, Fully developed mixed convection in horizontal and inclined tubes with uniform heat flux using nanofluid, Int. J. Heat Fluid Flow, 29 (2008) 545–556.

[17] A. Akbarinia, A. Behzadmehr, Numerical study of laminar mixed convection of a nanofluid in a horizontal curved tube, Appl. Therm. Eng., 27 (2007) 1327–1337.

[18] R. Lotfi, Y. Saboohi, A.M. Rashidi, Numerical study of forced convective heat transfer of nanofluids: comparison of different approaches, Int. Commun. Heat Mass Transf., 37 (2010) 74–78.

[19] R.M. Moghari, A.S. Mujumdar, M. Shariat, F. Talebi, S.M. Sajjadi, A. Akbarinia, Investigation effect of nanoparticle mean diameter on mixed convection Al_2O_3-water nanofluid flow in an annulus by two phase mixture model, Int. Commun. Heat Mass Transf., 49 (2013) 25–35.

[20] A. Akbarinia, R. Laur, Investigation the diameter of solid particles affects on a laminar nanofluid flow in a curved tube using a two phase approach, Int. J. Heat Fluid Flow, 30 (2009) 706–714.

[21] S. Mirmasoumi, A. Behzadmehr, Numerical study of laminar mixed convection of a nanofluid in a horizontal tube using two-phase mixture model, Appl. Therm. Eng., 28 (2008) 717–727.

[22] Y. Abbassi, A.S. Shirani, Sh. Asgarian, Two-phase mixture simulation of Al_2O_3/water nanofluid heat transfer in a non-uniform heat addition test section, Progress in Nuclear Energy, 83 (2015) 356–364.

[23] A. Behzadmehr, M. Saffar-Avval, N. Galanis, Prediction of turbulent forced convection of a nanofluid in a tube with uniform heat flux using a two phase approach, Int. J. Heat Fluid Flow, 28 (2007) 211–219.

[24] O. Ghaffari, A. Behzadmehr, H. Ajam, Turbulent mixed convection of a nanofluid in a horizontal curved tube using a two-phase approach, Int. Commun. Heat Mass Transf., 37 (2010) 1551–1558.

[25] S.M. Izadi, A. Behzadmehr, D. Jalali-Vahida, Numerical study of developing laminar forced convection of a nanofluid in an annulus, Int. J. Therm. Sci., 48 (2009) 2119–2129.

[26] R.M. Moghari, A. Akbarinia, M. Shariat, F. Talebi, R. Laur, Two phase mixed convection Al_2O_3–water nanofluid flow in an annulus, Int. J. Multiph. Flow, 37 (2011) 585–595.

[27] T. Tayebi, A.J. Chamkha, Natural convection enhancement in an eccentric horizontal cylindrical annulus using hybrid nanofluids, Numerical Heat Transf.: Part A, 71 (2017) 1159–1173.

[28] O. Mahian, S. Mahmud, S. Wongwises, Entropy generation between two rotating cylinders with magnetohydrodynamic flow using nanofluids, J. Thermophys Heat Transf., 27 (2013) 161–169.

[29] O. Mahian, S. Mahmud, S. Zeinali Heris, Effect of uncertainties in physical properties on entropy generation between two rotating cylinders with nanofluids, J. Heat. Transf., 134 (2012) 101704 (9 pages).

[30] O. Mahian, S. Mahmud, S. Zeinali Heris, Analysis of entropy generation between corotating cylinders using nanofluids, Energy, 44 (2012) 438–446.

[31] O. Mahian, A. Kianifar, C. Kleinstreuer, M.A. Al-Nimr, I. Pop, A.Z. Sahin, S.Wongwises, A review of entropy generation in nanofluid flow, Int. J. Heat Mass Transf., 65 (2013) 514–532.

[32] V. Bianco, O. Manca, S. Nardini, Performance analysis of turbulent convection heat transfer of Al_2O_3 water-nanofluid in circular tubes at constant wall temperature, Energy, 77 (2014) 403-413.

[33] M. Bahiraei, S. Mohammadi Majd, Prediction of entropy generation for nanofluid flow through a triangular minichannel using neural network, Adv. Powder Technol., 27 (2016) 673–683.

[34] M. Manninen, V. Taivassalo, S. Kallio, On the mixture model for multiphase flow, VTT Publications 288, Technical Research Center of Finland, 1996.

[35] L. Schiller, A. Naumann, A drag coefficient correlation, Z. Ver. Dtsch. Ing., 77 (1935) 318–320.

[36] N. Masoumi, N. Sohrabi, A. Behzadmehr, A new model for calculating the effective viscosity of nanofluids, J. Phys. D. Appl. Phys., 42 (2009) 055501.

[37] C.H. Chon, K.D. Kihm, S.P. Lee, S.U.S.Choi, Empirical correlation finding the role of temperature and particle size for nanofluid (Al_2O_3) thermal conductivity enhancement, J. Appl. Phys., 87 (2005) 153107 (3 pages).

[38] M. Soltani, P. Chen, Shape design of internal flow with minimum pressure loss, Adv. Sci. Let., 2 (2009) 347–55.

[39] Y. Sheikhnejad, R. Hosseini, M. Saffar Avval, Experimental study on heat transfer enhancement of laminar ferrofluid flow in horizontal tube partially filled porous media under fixed parallel magnet bars, J. Magn. Magn. Mater. 424 (2017) 16–25.

Graphical Abstract